

Preliminary design optimization of a fully superconducting motor based on disk-up-down-assembly magnets

Rui Wang, Yingzhen Liu, Jiwei Cao, Liyi Li, Xiaokun Liu, Haida Xue, Tabea Arndt

Abstract—The transition to electric propulsion for aircraft provides an effective way to reduce fuel consumption and achieves low-carbon aviation. Due to the advantages of high magnetic field and ultra-compactness of superconducting disk-up-down-assembly (‘DUDA’) magnets, they have a promising use in superconducting motors. Therefore, this paper presents a design of a fully superconducting motor using superconducting DUDA magnets with Halbach arrays. In order to study the feasibility of the superconducting DUDA magnets in electric motors, preliminary studies of two sets of 4-layer superconducting DUDA magnets were carried out. The manufacturing method with lap joints of the DUDA magnets was proposed and then the manufactured magnets were tested in liquid nitrogen. The contact resistance and critical current at each lap joint have been calculated and the magnetic field distribution of the magnets has been measured. The magnetic fields of the magnets were also verified by simulation and then the magnets were scaled up in size to meet the magnetic field magnitude for the motor. It has been proved that the DUDA magnets can generate a constant magnetic field above 1.11 T along the x -axis without iron materials, which meets the requirements of motors.

Based on the analysis of electromagnetic performance, the structural parameters of the superconducting DUDA magnets were optimized with different pole-slot number combination in order to obtain higher efficiency and specific power density. To calculate the efficiency, finite element models in Comsol evaluated the AC losses of the superconducting DUDA magnets. By changing the slot type and winding configuration, the optimized motor is able to achieve a specific power density of 11.55 kW/kg with an efficiency of 98% at 30 K.

Index Terms—superconducting DUDA magnets, Halbach arrays, fully superconducting motor, contact resistance, critical current, specific power density, AC losses.

I. INTRODUCTION

Rapid development of air traffic is increasing fossil fuel consumption and greenhouse gases emissions. Previous studies show that electric propulsion in aircraft offers an effective route to reducing fuel consumption and achieving low carbon aviation, even zero emissions [1]-[3]. To enable electric aircraft, motors with high specific power density and high efficiency are necessary. Fig. 1 listed the specific power density of motors for electric aircraft in literature [4]-[13]. Some of the motors in Fig. 1 are only conceptual designs or demonstrators, especially for superconducting motors. It can be concluded that superconducting motor technology is a promising solution for achieving a specific power density over 15 kW/kg, which meets the requirement for commercial aircraft [14]. In 2021 A Yak-40LL driven by a 500 kW superconducting motor was first demonstrated in flight in Moscow, which proves superconducting motor technology is not only promising in conceptual designs, but also feasible for real electric aircraft. Moreover, Airbus is exploring the potential to employ superconductivity and cryogenics for aircraft in the ASCEND project, in which superconducting motors and cables are key components.

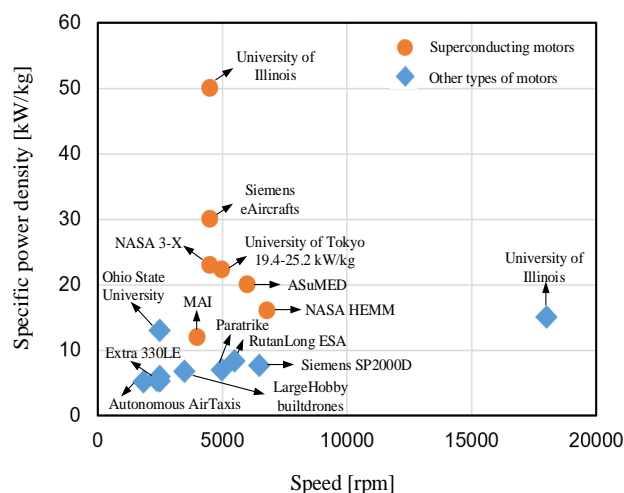


Fig. 1. Specific power density of motors for electric aircraft.

In superconducting motors, superconducting magnets are important for power conversion. They are generally located in the rotor as the magnetic poles. Up to now, the most widely used superconducting magnets in motors are wound coils [5][15]. The technology to manufacture the wound superconducting coils is quite advanced. However, in order to produce high magnetic fields, the number of turns of the magnets is large and it is very difficult to guarantee a homogeneous critical current

distribution along tape length. This will lead to a waste of tape ability since the critical current of the superconducting coil, as well as the operating current, is determined by the lowest critical current of the tapes. In addition, the inhomogeneity along the length can cause deviations between the design and experiments [16]. Furthermore, the minimal bending diameter will limit the superconducting coil size and compactness. In order to transport DC current from a power source, current leads are needed and losses are introduced to the magnet system.

To avoid the current leads, to reduce the magnet space, and to simplify the manufacture process, superconducting stack and bulk magnets for electric motors have been developed. The stack and bulk magnets can trap magnetic field by pinning effects, and produce a field larger than permanent magnets by using the pulsed field method or field cooling method of magnetization. A superconducting rotating motor with bulk and stack magnets, was proposed in [17] and [18]-[20], respectively, which proves that bulk and stack magnets are feasible to achieve a compact and high-torque rotating machine. Similar to the stack magnet, the ring magnet, made of split tapes stacked together, is proposed for achieving a higher magnetic field, and it is a closed-loop magnet without the metal contact from one turn to the other [22]. However, the field stability of the superconducting bulk and stack magnets is a severe issue to tackle, since they are faced with demagnetization problems due to the time-varying magnetic field fluctuations from the stator [23],[24]. Unlike the wound superconducting coils, the field of bulks and stacks cannot be controlled during the motor operation.

In order to take advantages of the aforementioned three types of superconducting magnets, a new concept, named as disk-up-down-assembly ('DUDA'), was developed from the widely used copper Bitter magnets in high field areas and was initially proposed by T. Arndt from Karlsruhe Institute of Technology (KIT), as shown in Fig. 2 [25]. Short superconducting tapes are first cut or manufactured in a rectangular or circular shape with a slit. The superconducting magnet consists of a stack of such rectangular or circular tapes and a thin sheet of insulation, similar to the copper Bitter magnets, separates each tape. These slits allow the current to flow from one superconducting tape to the other through the overlapped region by soldering or superconducting joints. Then the current can flow from one end of the stack to the other end, and magnetic fields are generated. In order to make the resistance of contacts as small as possible, the superconducting layers in the tapes are soldered together to avoid current passing through substrates and buffer layers.

With a constant power supply, the magnetic field generated by the superconducting DUDA magnets is stable under the transient operations of motors. There is no demagnetization and the field is controllable. Since the required single tape length is small, the homogeneity of critical current along tape length can be guaranteed and the manufacture cost of the tape will be reduced due to a shorter piece length. As there is no limit of minimal bending diameter, the magnet can be extremely compact. As a result, compact Halbach magnet arrays for superconducting motors can be realized. This enables a stronger magnetic field to be created inside the Halbach arrays and a weaker magnetic field outside, which increases the magnetic field in the air-gap and enables an ironless rotor in rotating machines. In this way, the weight of the rotating machines can be reduced and the specific power density is increased.

In this paper a new concept of the superconducting magnet for electric motors is proposed, which is compact, stable and controllable in magnetic field and simple to manufacture. The work here is to study the benefits of utilizing the proposed DUDA magnets to the superconducting motors and is organized as follows. The background and the motivation of the work are introduced in Section I. In Section II, the manufacturing method and electro-magnetic performance of the DUDA magnets are investigated, followed by the evaluation of the magnetic field of a scale-up magnet through simulation to meet the requirements of an actual motor. Moreover, the design optimization of a superconducting motor with Halbach arrays of DUDA magnets is presented in Section III. The results and findings are then summarized in Section IV.

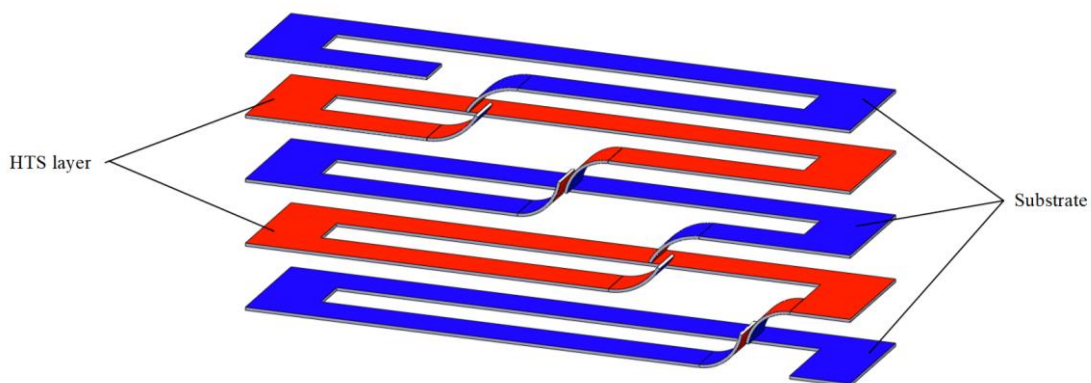


Fig. 2. Superconducting DUDA magnets for electric motors (red: HTS layer, blue: Substrate).

II. MANUFACTURING METHOD AND ELECTRO-MAGNETIC PERFORMANCE OF THE DUDA MAGNETS

In order to study the benefits and feasibility of the DUDA magnets to motors, proof-of-principle studies are first carried out and the manufacturing method of the DUDA magnets for motors is proposed. For radial flux motors, superconducting tapes in rectangular shapes are used. The length of each superconducting tape is the same as the motor axial stack length, which is typically within the range of one meter for MW-class motors. The width of superconducting tapes for DUDA magnets

is determined by motor designs. Currently, the most widely used tapes in the market are 4-12 mm in width, and the width of commercial superconducting tapes is increasing, which gives more design options for the DUDA magnets in motor application. For instance, Shang Creative Superconductor Technologies and American Superconductor Corporation can produce 20 mm and 40 mm high temperature superconducting tapes by the metal-organic deposition (MOD) method. Other tape manufacturers are to follow, for example SuNAM. To start with a very easy experimental setup, superconducting tapes from the Shang Creative Superconductor Technologies are used to prepare the DUDA magnets and liquid nitrogen is used for cooling.

A. Structure of the DUDA Magnets and the Manufacturing Method

To manufacture the superconducting DUDA magnets, superconducting face-to-face lap joints are employed. Two sets of 4-layer DUDA magnets with YBCO tapes are manufactured. The structural parameters and critical current density curves of the superconducting tapes at 30 K and 77 K provided by the Shang Creative Superconductor Technologies are shown in Table I and Fig. 3. The critical current density of the superconducting tapes at self-field, 77 K is 131.9 A/mm².

Fig. 4(a) shows a schematic drawing of the soldered structure of the superconducting magnets, where the red parts are the superconducting layers of the superconducting tapes, the yellow parts are the substrate layers, and the purple parts are the interlayer spacers. The interlayer spacers are used to ensure a flat soldering surface between the superconducting tapes. Before soldering, both sides of the superconducting tapes are pasted with insulation layers except the region for the lap joints. The superconducting layers of two adjacent superconducting tapes are soldered to each other with an overlap length and width of 10 mm and 4.5 mm respectively. The length of the upper most and lower most tape of the DUDA magnet is 73 mm, which is longer than the other tapes for current lead connections.

Fig. 5 shows the pressure device for the soldering process. The stacked superconducting magnets with InAg3-solder, insulation and interlayer spacers are placed into the device first. Aluminum nitride ceramic is used for the interlayer spacers due to its high thermal conductivity. Then the steel bolts are screwed to apply pressure to the soldering joints. The pressure used to prepare the DUDA magnets is 0.5 MPa. A temperature sensor is connected to the base part of the pressure device. The whole set is then placed in a thermostat for heating up to a temperature of 170 °C. The specific soldering parameters are shown in Table II. A picture of the prepared superconducting DUDA magnet is shown in Fig. 4(b).

Table I. Specification of superconducting tapes

Parameter	Value
Type	YBCO
Width	13 mm
Thickness	0.28 mm
Length	60 mm/73 mm
Critical current density	131.9 A/mm ² (77 K)
Overlap width	4.5 mm
Overlap length	10 mm

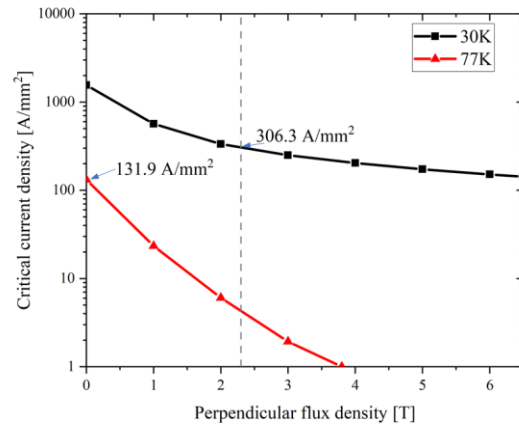
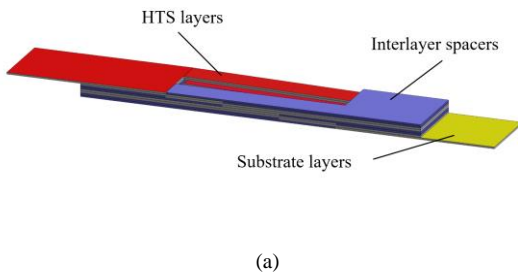
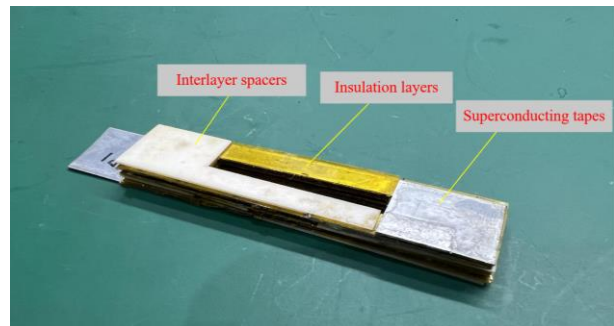


Fig. 3. Critical current density of the superconducting tape provided by the Shang Creative Superconductor Technologies.



(a)



(b)

Fig. 4. The structure of the superconducting DUDA magnets, (a) schematic drawing and (b) experimental picture.

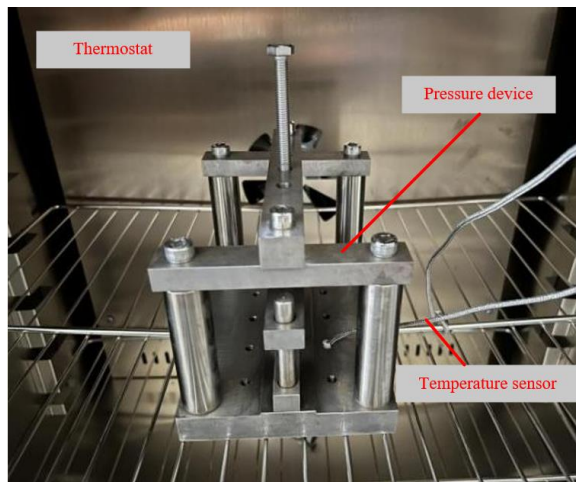


Fig. 5. Pressure device for the soldering process.

Parameter	Value
Soldering material	In-Ag3
Temperature	170 °C
Pressure	0.5 MPa
Interlayer spacer material	Aluminum nitride ceramic

B. Critical Current and Contact Resistance

The measurement device for superconducting DUDA magnets in liquid nitrogen is shown in Fig. 6. Measurement wires for voltage are connected on both sides of each lap joint of the soldered DUDA magnet. To calculate the lap resistance and critical current, the voltage and current curves ($V-I$) are recorded and Hall probes are placed at different locations on the magnet surface to measure the magnetic field distribution.

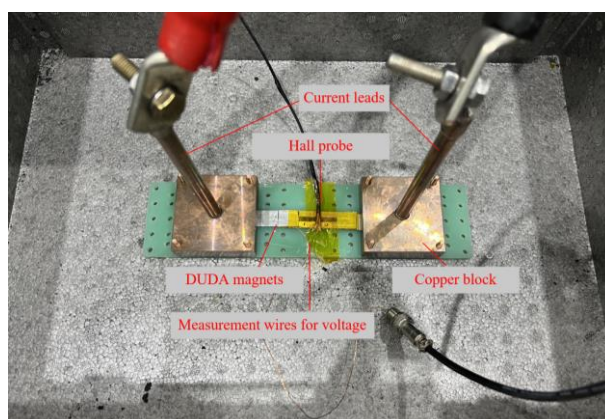


Fig. 6. Device for contact resistance and critical current measurement.

The measurement device is immersed in liquid nitrogen and the supplied current is increased gradually. The corresponding voltage of each lap joint is recorded, as shown in Fig. 7. A-1, A-2, and A-3 are the three lap joints of the first DUDA magnet, and B-1, B-2, and B-3 are the three lap joints of the second DUDA magnet.

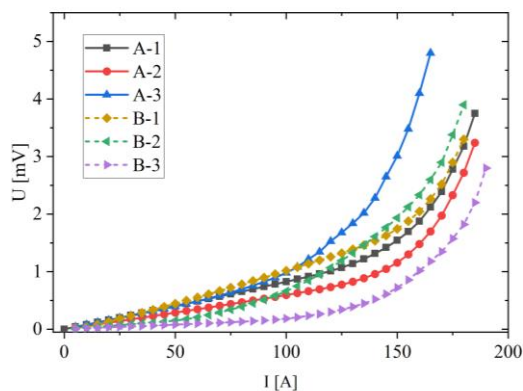


Fig. 7. Measured voltage-current curves for all lap joints.

For the soldering joints of the YBCO tapes, due to the zero resistance of superconducting layers, when the current flowing through the joints is less than the critical current, the voltage-current ($U-I$) curve of each lap joint measured by the four-wire method should be linear, and the slope of the curve is the contact resistance of the soldering joints. When the current flowing

through the joints reaches or is greater than the critical current, the YBCO tape is no longer non-resistive and will produce a high voltage. Therefore, the expression of the contact resistance can be approximated as follows:

$$\begin{cases} U = RI, I < I_c \\ U = RI + E_c d \left(\frac{I}{I_c} \right)^n + C, I \geq I_c \end{cases} \quad (1)$$

where E_c is the criterion of superconducting to normal state transition, generally $1 \mu\text{V}/\text{cm}$, d is the distance between the two voltage wires, I_c is the critical current, n is the transition sharpness of the YBCO tapes from superconducting to normal state, R is the contact resistance and C is the error correction factor.

Through the mathematical fitting of equation (1), the contact resistance R and critical current I_c of each lap joint of the two sets of magnets can be obtained, as shown in Table III. The contact resistance of joint A-1 is largest, which is $9.72 \mu\Omega$. The contact resistance of joint B-3 is the smallest, which is $1.40 \mu\Omega$.

Joints	Resistance ($\mu\Omega$)	Critical current density (A/mm^2)	Percentage decrease
A-1	7.70	99.20	24.76%
A-2	5.39	97.62	25.97%
A-3	9.24	73.01	44.63%
B-1	9.72	101.59	22.96%
B-2	6.16	59.52	54.86%
B-3	1.40	96.03	27.17%

The advantage of superconducting DUDA magnets is that they have a compact structure, and when the superconducting tape width and the number of stacked layers increase, the magnet can produce a higher magnetic field. However, the two main aspects that currently affect the performance of the magnet are the critical current of the superconducting magnets and the contact resistances of the lap joints. In our preparation of the DUDA magnets, in order to get the superconducting tape into a rectangular shape, laser cutting is used. During the cutting, there might be too much energy from the laser which can damage the surface of the tapes. Moreover, due to the multi-layer structure of superconducting tapes, different layers are subjected to different thermal deformations, and the heating process for soldering the magnet can lead to delamination [26]. As a result, the critical current of the magnet is decreased due to the delamination after the manufacturing process, as listed in Table III. According to the literature, the lowest contact resistance of the face-to-face superconducting lap joints can reach $10^{-8} \Omega$ [27], which is much smaller than what we have obtained. One reason is the delamination of the superconducting tapes as aforementioned. The other reason lies in the value of the applied soldering pressure and the homogeneity of the soldering pressure for each lap joint. Since the lap joints in the DUDA magnet are stacked along the spiral direction, the homogeneity of the applied pressure on each lap joint depends on the flatness of the soldering plane. More effort is required to avoid delamination of the tape and to decrease the joint contact resistance.

C. Magnetic Field

The magnetic field distribution of the DUDA magnet is measured. The measurements are taken at the center of the long side of the magnet and 4.0 mm from the magnet surface in order to fix the hall probe on the magnet, and the specific measurement points are shown in Fig. 8.

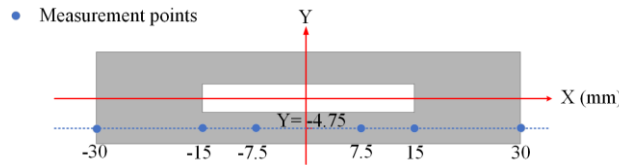


Fig. 8. Schematic diagram of the positions in the magnetic field measurement.

Meanwhile, the DUDA magnet is simulated with the same dimensions by finite element software *Comsol 5.6* with the physics of magnetic field, in which the magnetic vector potential is the main variable and the operating current density distribution is assumed to be uniform in the tape [16]. When the current density of the magnet is $96 \text{ A}/\text{mm}^2$ (the current provided is 120.96 A), the curve of the simulated and measured magnetic field distribution are shown in Fig. 9. It can be seen that the measured and simulated magnetic field distribution are consistent with a value of 13.9 mT at the center. We then used the same simulation model to predict the centered magnetic field distribution of the DUDA magnet along the x -axis in Fig. 8. The centered magnetic field distribution is also drawn in Fig. 9. It can be proved that the DUDA magnet can produce a constant magnetic field along the x -axis with a value of 17.4 mT at the center, except for the region close the end winding.

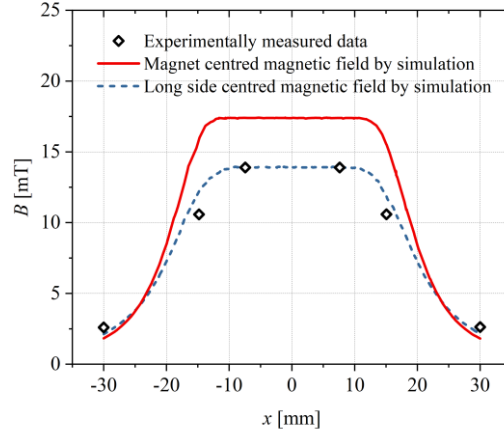


Fig. 9. Magnetic field distribution of superconducting DUDA magnets (4 mm from the upper surface of the magnet).

Due to the limitations of the available width of the superconducting tapes and the manufactured components for the DUDA magnets, we scaled-up the simulation model of the DUDA magnet to a width of 20 mm, a length of 100 mm and a stacking thickness of 20 mm to evaluate whether this type of magnet is satisfactory for applications in motors. The critical current density of 306.3 A/mm^2 at temperature of 30 K and at an external magnetic field of 2.3 T from Fig. 3 is assumed as the current density in the simulation, which is within a typical field range in superconducting rotating motors. In aviation, liquid hydrogen is considered as a fuel. The boiling point of liquid hydrogen at 1 bar is about 21 K. When using a fuel-cooling circuit with higher pressure, one has to consider a slightly increased temperature; the temperature gradient along a cooling bus may add some additional Kelvin to the boiling point, so an operating temperature of 30 K accounts for these effects and provides a practical temperature margin for safe operation.

The magnetic field distribution of a scaled magnet was analyzed first. Fig. 10 shows the amplitude of the magnetic field distribution at 2 mm from the upper surface of the magnet ($z = 12 \text{ mm}$). The z -component of the central magnetic field of the magnet along the x -axis is presented in Fig. 11, from which it can be seen that the z -component of the central magnetic field generated by the DUDA magnet increases substantially after enlarging the magnet and the supplied current density. The z -component of the magnetic field at $z = 12 \text{ mm}$ was investigated, since this will be the radial component of the air-gap magnetic field for torque generation in a motor.

Subsequently five DUDA magnets with the same parameters were combined into Halbach arrays. The distribution of the magnetic field and magnetic flux lines of the magnets in the yz -plane at $x = 0 \text{ mm}$ is shown in Fig. 12. The magnetic field is strengthened in the positive z -direction and the field is weakened in the negative z -direction, similar to the Halbach arrays in electric motors. A yellow dashed line at $z = 12 \text{ mm}$ in this yz -plane is selected to draw the z -component magnetic field distribution of the array in the y -axis, as shown in Fig. 13(a). The z -component of the magnetic field generated by this Halbach array is in a sinusoidal distribution and the maximum field is 1.11 T. Three points in Fig. 12 are selected to draw the magnetic field distribution along the x -axis and the results are shown in Fig. 13(b). The z -components of the magnetic field of the three points can represent a $1/4$ period of the field distribution along the y -axis as illustrated in Fig. 13(a). Fig. 13(b) shows that the z -components of the magnetic field of all three points can produce a constant magnetic field along the x -axis.

From the above simulation results of the two scaled models, it can be concluded that the Halbach arrays consisting of DUDA magnets generate a constant magnetic field along the x -axis and produce a periodic sinusoidal magnetic field along the y -axis, which meets the requirements of the field distribution in a motor. The maximum z -component of the magnetic field generated by the Halbach arrays is 1.11 T. This is limited by the current-carrying ability of the tapes used. If the critical current density of the superconducting tapes is increased to $I_c = 725 \text{ A/mm}^2$ at 30 K, 3 T, as presented in [25], the Halbach array can generate a magnetic field of 2.65 T at 2 mm from the upper surface of the magnets. These field values are suitable for the air-gap magnetic field in electric motors. Furthermore, by employing iron materials, the magnetic field generated by the Halbach arrays can be increased. To utilize the superconducting DUDA magnets and to investigate the potential benefits, a superconducting motor with Halbach arrays of DUDA magnets is designed in the following section.

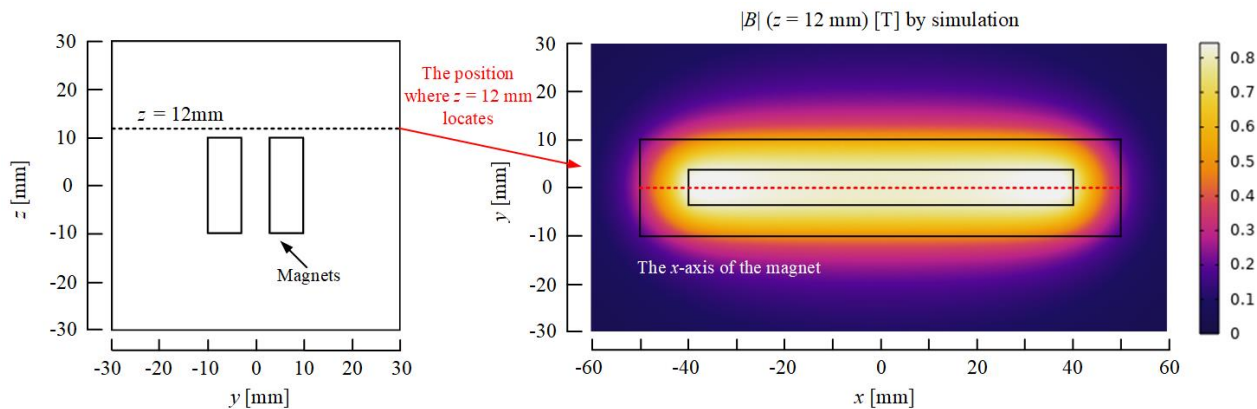


Fig. 10. Simulated distribution of the z -component of the magnetic field of a DUDA magnet in the xy -plane (2 mm from the upper surface of the magnet; $z = 12$ mm).

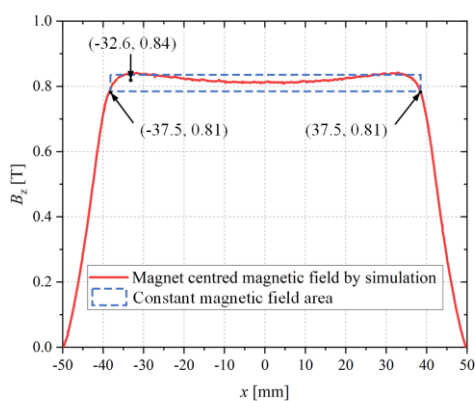


Fig. 11. Simulated distribution of the z -component of the central magnetic field of a DUDA magnet along the x -axis (2 mm from the upper surface of the magnet; $z = 12$ mm).

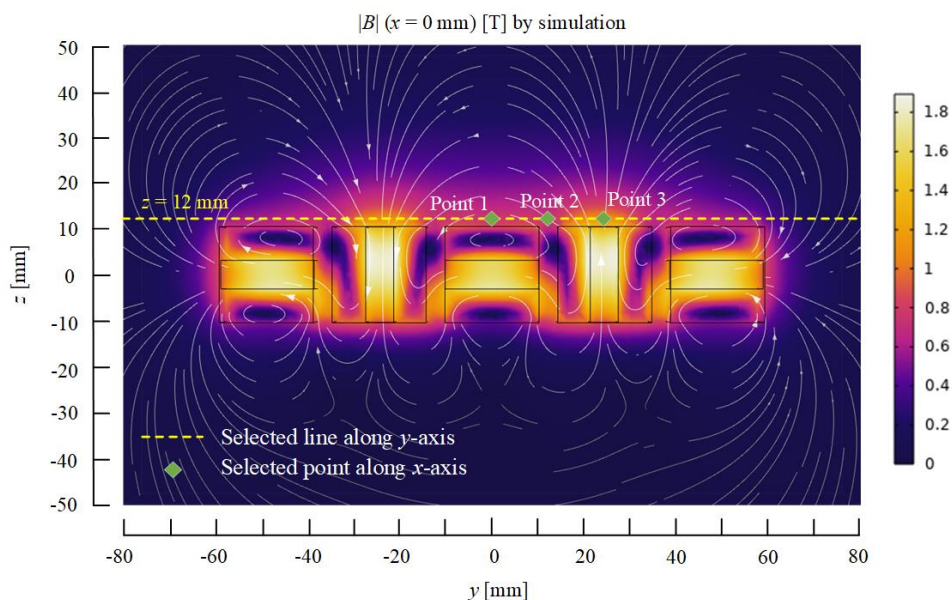


Fig. 12. Simulated distribution of the magnetic field in the yz -plane for a Halbach array consisting of five DUDA magnets.

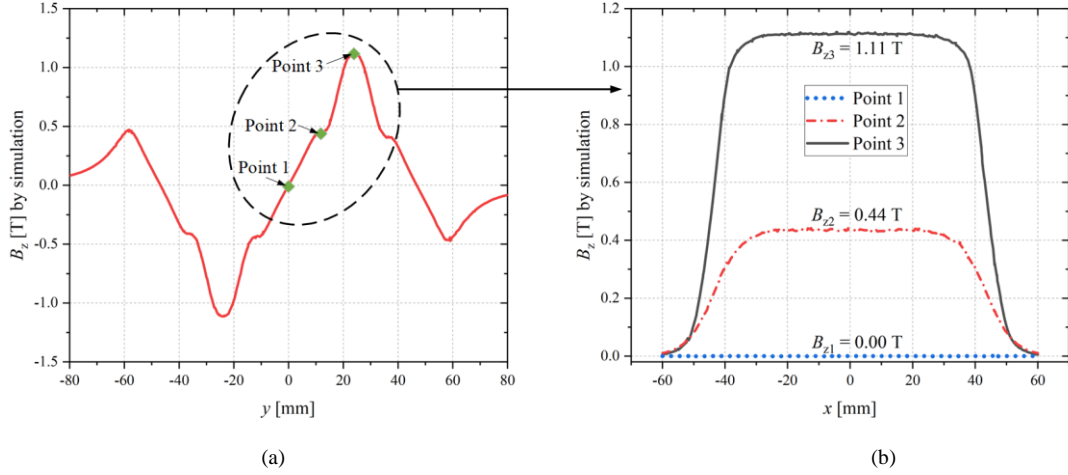


Fig. 13. Simulated magnetic field distribution of the DUDA magnet in a Halbach array in different axes, (a) Magnetic field distribution along the y -axis ($x = 0$ mm, $z = 12$ mm) and (b) Magnetic field distribution of the three points along the x -axis (the three points represent a $1/4$ period of the spatial distribution in a motor).

III. DESIGN OF SUPERCONDUCTING MOTORS WITH HALBACH ARRAYS OF DUDA MAGNETS

A. Structure of the Proposed Motor

Fig. 14 shows the general structure of the superconducting motor. From inside to outside, it mainly consists of a stator core, superconducting armature coils, superconducting DUDA magnets, and a non-magnetic rotor core. In order to increase the magnetic loading and torque, the motor has an external rotor structure. The superconducting armature coils in the stator are wound by superconducting tapes. Superconducting DUDA magnets arranged in Halbach arrays are used in the rotor to increase the magnetic flux density in the air-gap and to reduce it in the rotor core, which can enable an ironless rotor and decrease the weight of the rotor. A cobalt iron core is used for the inner stator to allow a higher saturation field of 2.35 T.

The schematic drawing of the DUDA magnets in cross-section is shown in Fig. 15. A unit of DUDA magnets consists of magnet A and magnet B. Where W_1 is the width of superconducting magnet A, L_1 is the stack length of superconducting magnet A, d_1 is the width of each side of magnet A after cutting, W_2 is the width of superconducting magnet B, L_2 is the stack length of superconducting magnet B, d_2 is the width of each side of magnet B after cutting.

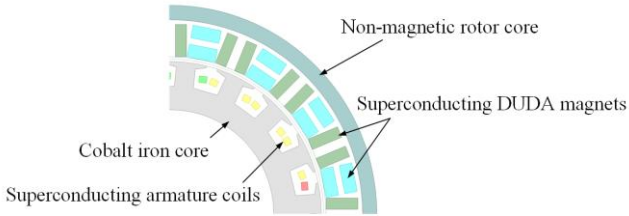


Fig. 14. The structure of the proposed fully superconducting motor with Halbach arrays.

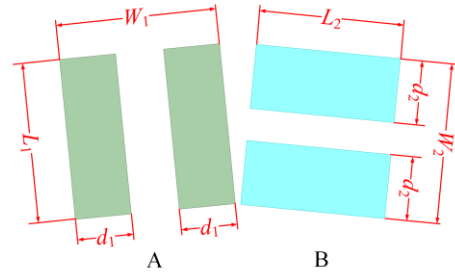


Fig. 15. The cross-sectional diagram of the DUDA magnets.

B. Modelling Method

A rated power of 1 MW, a rated speed of 6000 rpm, and a rated efficiency of 98% are selected as the design targets in this paper. The air-gap diameter of the motor is selected to be 194 mm for a compact design. The physical air-gap length is 4 mm, since the stator and rotor are in the same vacuum Dewar. By taking the space for stator cooling system into consideration, the inner diameter of the stator is determined to be 130 mm. The operating temperature of both the superconducting armature coils in the stator and the superconducting DUDA magnets in the rotor is 30 K, while the stator core is uncooled. A temperature of 30 K can be achieved by a centralised cooling system with a closed hydrogen loop. The superconducting armature coils and the superconducting DUDA magnets are made of YBCO tapes, whose superconducting characteristics are shown in Fig. 3. The design specifications of the superconducting motor are listed in Table IV.

Since the maximum width of the currently available superconducting tapes is 40 mm, the width of magnet A, W_1 , and the width of magnet B, W_2 , are in the range of 15–40 mm. From Fig. 14 it can be seen that the rotor outer diameter is determined by the air-gap diameter and the width of magnet B. Then the circumferential length of the rotor and the width of magnet A will influence the options of the pole pair number. The slot number and dimensions in the stator are subject to the minimum span of the superconducting armature winding and air-gap diameter. The corresponding design range of the varied parameters of the superconducting motor are listed in Table V.

In this section, five different pole-slot number combinations were investigated with the same air-gap diameter: M1 represents motor design with 8 pole/9 slot, M2 represents 10 pole/9 slot, M3 represents 12 pole/9 slot, M4 represents 16 pole/18 slot, and M5 represents 20 pole/18 slot. The widths of the tapes were selected to be 40 mm for M1, 30 mm for M2, 25 mm for M3, 20 mm for M4 and 15 mm for M5. As the widths of the tapes for the different pole-slot number combinations have been determined, the widths of magnet A, W_1 , and magnet B, W_2 , have also been determined. Then, according to the widths of the magnets, the rotor outer diameters of the five designs are 304 mm, 284 mm, 274 mm, 264 mm and 254 mm. In order to ensure the same supplied current and current density in the armature coils of the motor with different pole-slot number combinations, the width of the armature coil tape for M1, M2 and M3 is 4 mm, and the width of the armature coils is 10 mm. The width of the armature coil tape for M4 and M5 is 4 mm, and the width of the armature coils is 5 mm.

In this section, the electromagnetic performances of the five motor designs were calculated through finite element software *Maxwell* with the magnetic vector potential as the dependent variable and the AC losses of the superconducting armature coils were evaluated through *Comsol 5.6* based on *T-A* formulation [15].

Table IV. The design specifications of the superconducting motor

Parameter	Value	Unit
Rated power	1	MW
Rated speed	6000	rpm
Efficiency	98%	-
Working temperature	30	K
Air-gap diameter	194	mm
Physical air-gap length	4	mm
Stator inner diameter	130	mm
Superconducting armature coils materials	YBCO	-
Superconducting DUDA magnets materials	YBCO	-

Table V. The design range of varied parameters for the superconducting motor

Parameter	M1	M2	M3	M4	M5	Unit
Width of superconducting magnets	40	30	25	20	15	mm
Width of superconducting tape for armature coils	4	4	4	4	4	mm
Width of superconducting armature coils	10	10	10	5	5	mm
Pole-slot number combinations	8/9	10/9	12/9	16/18	20/18	-
Rotor outer diameter	304	284	274	264	254	mm

C. Dimensions of the DUDA Magnets and Their Operating Current Density

The influences of the dimension parameters of the superconducting DUDA magnets on the electromagnetic performance of the motor were analyzed. When the stacking length L_1 of magnet A becomes larger, the air-gap flux density of the motor increases. However, the stacking length L_1 is limited by the rotor outer diameter, which is determined by the width of magnet B, W_2 . When the stacking length L_2 of magnet B becomes larger, the air-gap flux density of the motor increases, but the stacking length L_2 is limited by the circumferential length. Therefore, the width and height of magnets A and B were finally chosen to be the same to improve the electromagnetic performance of the motor within the space restrictions.

The width of magnet A after cutting, d_1 , is chosen as the variable, and the width of magnet B after cutting, d_2 , is changed correspondingly in order to keep the same the critical current density of magnets A and B in operation based on the field dependence of the superconductor critical current. The electromagnetic performance of the motor is optimized for different pole-slot number combinations. The variation curves of the fundamental amplitude of the air-gap flux density as a function of d_1 are obtained under no-load conditions, as shown in Fig. 16. The maximum points of the air-gap flux density are selected to determine the structural parameters of the superconducting magnets for each model, and the specific parameters are shown in Table VI.

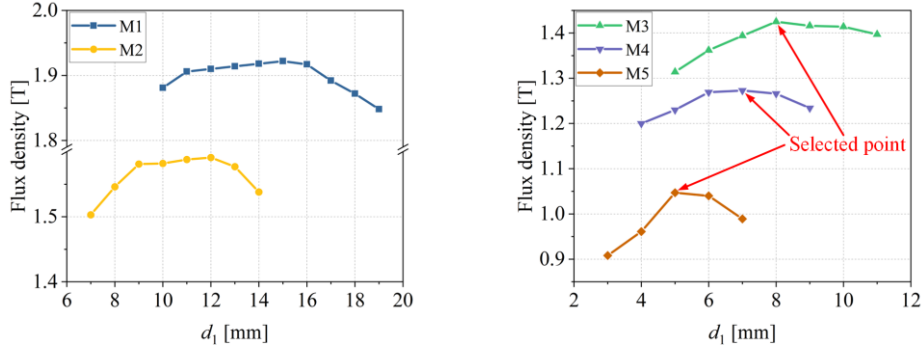


Fig. 16. Influence of the structural parameter of superconducting DUDA magnets d_1 on the air-gap flux density.

Table VI. Structural parameters of superconducting DUDA magnets with different pole-slot combinations

Pole-slot number combinations	W_1 (mm)	L_1 (mm)	d_1 (mm)	W_2 (mm)	L_2 (mm)	d_2 (mm)
8/9	40	40	15	40	40	18
10/9	30	30	12	30	30	13
12/9	25	25	8	25	25	10
16/18	20	20	7	20	20	8
20/18	15	15	5	15	15	6

The critical current of superconducting tapes has strong anisotropy. When the applied magnetic field is not parallel to the tape wider surface, the critical current of the superconducting tapes decreases rapidly. In addition, the critical current I_c drops the most when the magnetic field is perpendicular to the tape wider surface. Due to the structure of the proposed DUDA magnets, the maximum perpendicular field to the tape wider surface in the magnet is larger than the maximum parallel field. Therefore, the tape characterization data of the critical current I_c corresponding to the applied perpendicular field B_{\perp} can be used to determine the allowable excitation current for the DUDA magnets [28]. In order to ensure the stable operation of superconducting magnets and a reliable motor design, the maximum amplitude of the magnetic field in the DUDA magnets is used as the magnetic field to draw the magnet load line and a safety margin of 40% is adopted to the critical current.

The perpendicular field dependence of critical current density J_c-B_{\perp} of the superconducting tapes used in the magnets at 30 K is provided by the Shang Creative Superconductor Technologies, as shown in Fig. 3, and it is redrawn as the black curve in Fig. 17. The red curve represents the critical current with a safety margin of 40%. The intersection of the load line of the superconducting magnets in the motors and the J_c-B_{\perp} characteristic curve with 40% safety margin is selected as the operating current density of the DUDA magnets under no-load conditions, as shown in Table VII. The magnetic field distribution and peak magnetic flux density in the region of superconducting DUDA magnets at this current in the design of M1-M5 are shown in Fig. 18.

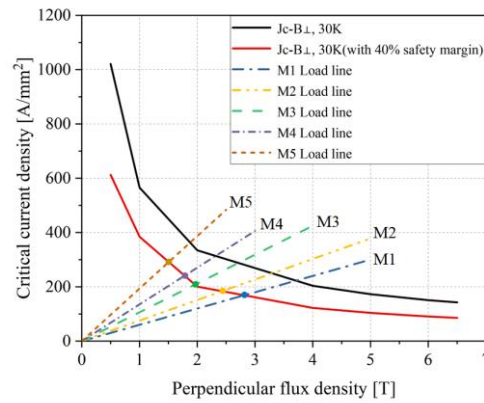


Fig. 17. Superconducting magnets J_c-B_{\perp} characteristics with load lines.

Table VII. The operating current density of superconducting DUDA magnets with different pole-slot combinations.

Pole-slot combinations	Operating current density (A/mm ²)
8/9	161
10/9	179
12/9	205
16/18	227
20/18	272

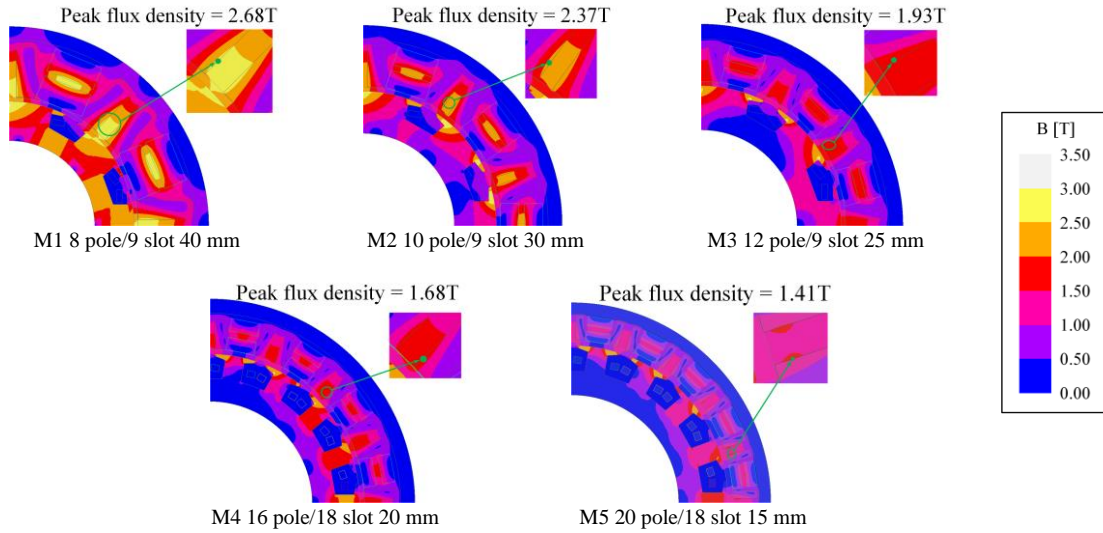


Fig. 18. Peak magnetic field in the region of superconducting DUDA magnets with different pole-slot number combinations.

D. Efficiency and Specific Power Density

The efficiency and specific power density of M1-M5 at different armature currents are analyzed in this section. In order to evaluate the efficiency of the different motor designs, the AC losses of the superconducting armature coils and iron losses are calculated using *Comsol 5.6*.

The equation for the overall efficiency of the motor is expressed as follows:

$$\eta = \frac{1}{P_N} \times \left(\frac{p_{dc} + p_{ac}}{\eta_{ce}} + p_s \right) \quad (2)$$

where p_{dc} is the DC loss of the DUDA magnets, p_{ac} is the AC loss of the armature coils, p_s is the stator core loss, P_N is the rated power of the motor, and η_{ce} is the cooling efficiency of cryogenic system. Since the theoretical contact resistance of the lap joints can be controlled in the range of 10 n Ω -100 n Ω [27], the percentage of DC losses will be very small and is not included in the efficiency calculation. The AC losses of the armature coils and the stator core loss are calculated by the simulation software.

Both DUDA magnets and armature coils operate at 30 K and the stator core is uncooled. When the machine losses at cold temperature is around 0.1%, the cryocooler power demand can reach 1% of the system power with a low temperature heat sink for the associated cryocooling system, when the operating temperature is in the range of 30-60 K [29]. Hence, in our paper, a factor of 10% is used to calculate the cryocooler power demand for cooling the AC loss of the armature coils at 30 K. The efficiency and specific power density as a function of armature current density for M1-M5 are shown in Fig. 19.

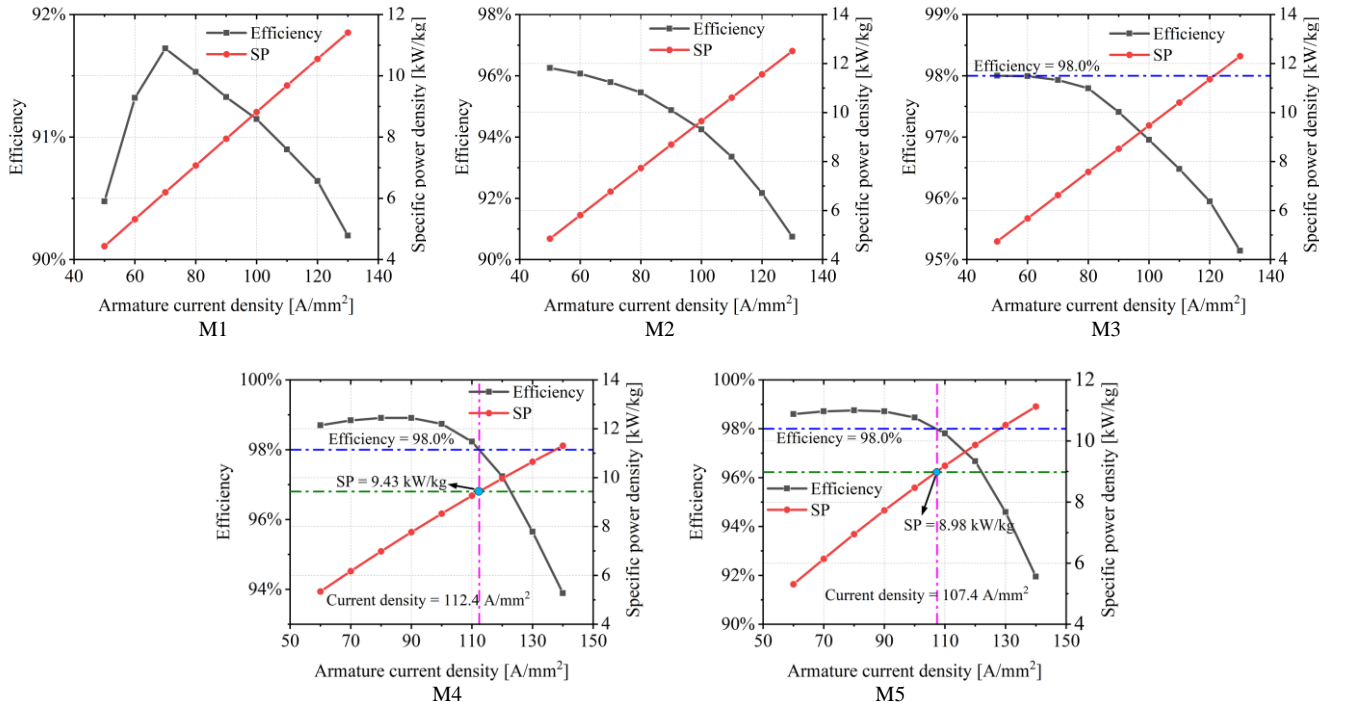


Fig. 19. Variation of motor efficiency and specific power density as a function of armature current density.

From Fig. 19, it can be observed that the efficiency of two motor designs M1 and M2 with 8 pole/9 slot and 10 pole/9 slot cannot satisfy the targeted efficiency of 98%. By comparing the specific power density of M3, M4 and M5 at an efficiency of 98%, it can be seen that the 16 pole/18 slot motor design has the highest specific power density, which is 9.43 kW/kg. Therefore 16 pole/18 slot was chosen as the optimal pole-slot number combination.

Fig. 20 shows the variation of the weight of each component of the motor as a function of the armature current density. The weight of the superconducting DUDA magnets, stator iron core, and the cryostat account for a relatively high proportion of the total weight. Therefore, to improve the specific power density of the motor, we need to improve the electromagnetic performance of the motor by increasing the air-gap flux density, and to reduce the weight of the materials used for each component at the same time.

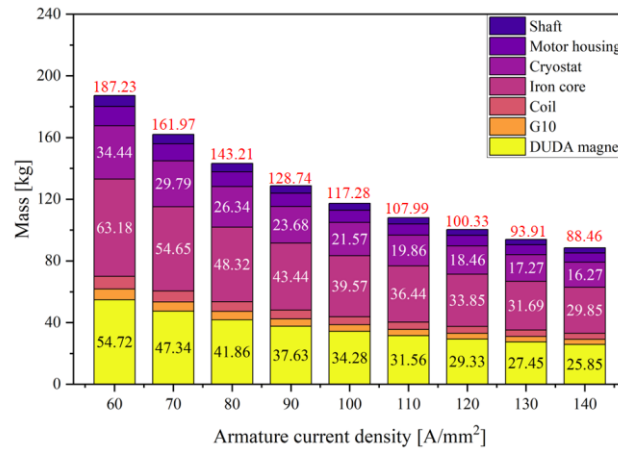


Fig. 20. Variation of the weight of each part of the motor as a function of armature current density.

As the width of the magnets from M1 to M5 decreases, the fundamental amplitude of the air-gap flux density also gradually decreases, as shown in Fig. 16. Therefore, the width of magnet A is increased and the stack length of magnet B is reduced, in order to increase the magnetic field produced by the magnets. The fundamental amplitude of the no-load air-gap flux density increases from 1.27 T to 1.30 T by increasing the width of magnet A to 30 mm and decreasing the stack length of magnet B to 8 mm. The effective cross-section area of a single unit of magnets is reduced from 600 mm² to 464 mm². The change of the magnets in the motor and their structural parameters are shown in Fig. 21.

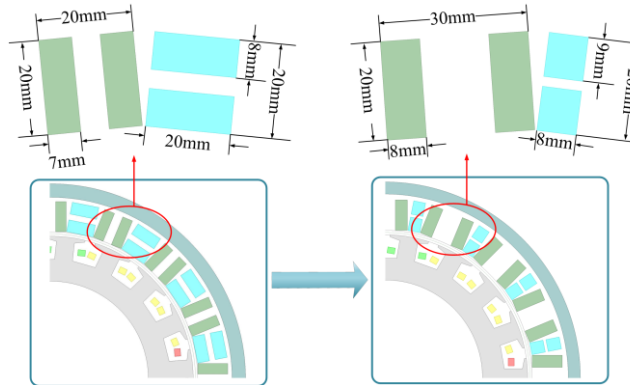


Fig. 21. Structural optimization of superconducting DUDA magnets.

In order to further reduce AC losses of the superconducting armature coils, the slot type and the height of armature coils of the motor were investigated. The parallel teeth were changed to parallel slots and the 4 mm wide coils changed to two 2 mm wide coils connected in parallel, as shown in Fig. 22.

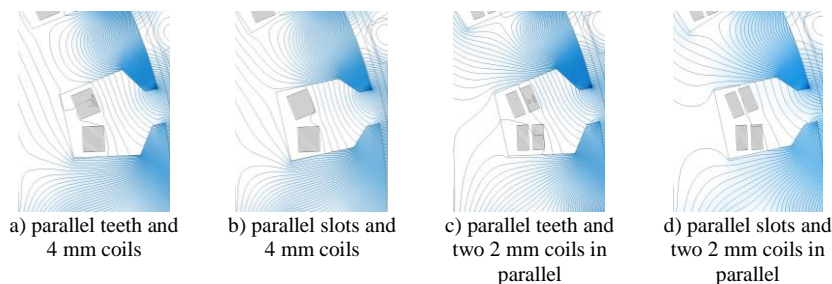


Fig. 22. Magnetic flux density and magnetic flux line distribution in stator slots.

By comparing the flux density in the superconducting armature coils as in Fig. 23 and the normalized current density as in Fig. 24, it can be seen that changing the slot type has a small effect on the maximum flux density of the superconducting armature coils, but can reduce the normalized current density. At the same time, changing the height of the superconducting armature coils has a small influence on the normalized current, but can reduce the maximum flux density.

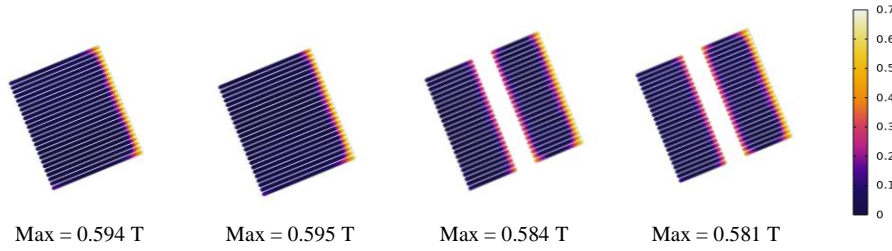


Fig. 23. Magnetic flux density.

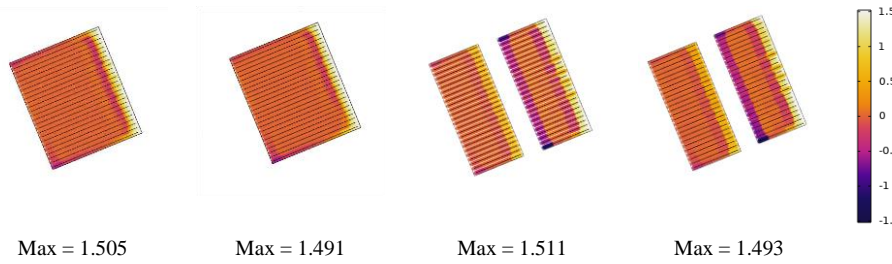


Fig. 24. Normalized current density J/J_c .

The AC losses of these four configurations were analyzed and the results are shown in Fig. 25. When the armature current density is in the range of 80-130 A/mm², the AC losses of the configuration with parallel slots and two 2 mm coils in parallel is the smallest. When the efficiency of the motor is 98%, the losses and the specific power of the four configurations in the stator are summarized in Table VIII.

All the four stator configurations with the optimized rotor from Fig. 21 can improve the specific power density of the motor with an efficiency of 98%. The configuration with parallel slots and two 2 mm coils in parallel reaches the highest specific power density, which is 11.55 kW/kg. It is 22.48% higher compared to the value of 9.43 kW/kg before the rotor is optimized.

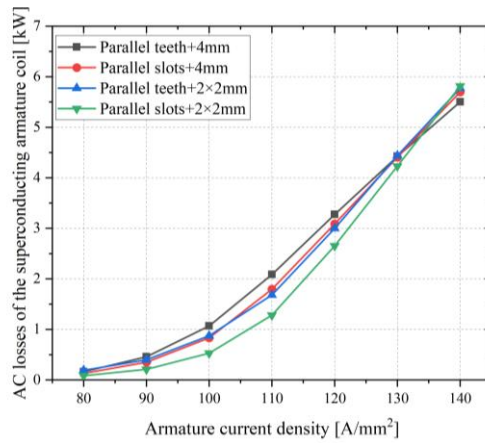


Fig. 25. AC losses of the superconducting armature coil as a function of armature current density.

Table VIII. The losses and specific power density of the four stator configurations when the efficiency is 98%

Plans	AC losses (W)	Iron losses (W)	Armature current density (A/mm ²)	Specific power density (kW/kg)
Parallel teeth and 4 mm coils	1302	6980	102.30	9.98
Parallel slots and 4 mm coils	1317	6830	105.04	10.32
Parallel teeth and 2x2mm coils	1348	6520	105.87	10.89
Parallel slots and 2x2mm coils	1384	6160	110.75	11.55

IV. CONCLUSION

In this paper a new structure of a fully superconducting motor with superconducting DUDA magnets in Halbach arrays is proposed. Preliminary studies on the DUDA magnets were carried out, including the manufacturing process, magnetic field, critical current and contact resistance of the lap joints in the DUDA magnets. Two 4-layer DUDA magnets were manufactured and the DUDA magnet can provide a stable magnetic field along the long side. When the magnets were scaled to a size that can be used in motors through simulations, the magnetic field of the DUDA magnets in Halbach arrays can be over 1.11 T. These results prove the feasibility of the proposed manufacturing method and the potential of the DUDA magnets for electric motors. However, more efforts are needed to improve the joint geometry, the soldering device, to optimize the laser cutting power and time, and to choose the appropriate soldering pressure and temperature in order to reduce the contact resistance and maintain the critical current. For future work having a larger area of lap joints is strongly recommended and locating them not in the direct current path, but only at one side of the coil stack, which provides better access and control of the preparation process. In addition, techniques to manufacture superconducting tapes into the required shape other than laser cutting are also worthy of investigating.

The designed motor was optimized in terms of efficiency and specific power density. The effect of the critical current of the pole-slot number combination, the geometry parameters of the DUDA magnets, slot type and height of the superconducting armature coils on the motor performance was investigated. The optimized design shows that by using Halbach arrays of superconducting DUDA magnets, the superconducting motor can reach a specific power density of 11.55 kW/kg with an efficiency of 98% at liquid hydrogen temperature. The superconducting DUDA magnets are compact and can provide promising magnetic fields, offering new opportunities for the development of superconducting motors.

REFERENCES

- [1] S. Sahoo, X. Zhao, and K. Kyrianiadis, "A Review of Concepts, Benefits, and Challenges for Future Electrical Propulsion-Based Aircraft," *Aerospace*, vol. 7, no. 4, p. 44, Apr. 2020, doi: [10.3390/aerospace7040044](https://doi.org/10.3390/aerospace7040044).
- [2] M. A. Rendón, C. D. Sánchez R., J. Gallo M., and A. H. Anzai, "Aircraft Hybrid-Electric Propulsion: Development Trends, Challenges and Opportunities," *J Control Autom Electr Syst*, vol. 32, no. 5, pp. 1244–1268, Oct. 2021, doi: [10.1007/s40313-021-00740-x](https://doi.org/10.1007/s40313-021-00740-x).
- [3] R. C. Bolam, Y. Vagapov, and A. Anuchin, "Review of Electrically Powered Propulsion for Aircraft," in *2018 53rd International Universities Power Engineering Conference (UPEC)*, Glasgow, Sep. 2018, pp. 1–6. doi: [10.1109/UPEC.2018.8541945](https://doi.org/10.1109/UPEC.2018.8541945).
- [4] T. Balachandran, D. Lee, N. Salk, and K. S. Haran, "A fully superconducting air-core machine for aircraft propulsion," *IOP Conf. Ser.: Mater. Sci. Eng.*, vol. 756, p. 012030, Jun. 2020, doi: [10.1088/1757-899X/756/1/012030](https://doi.org/10.1088/1757-899X/756/1/012030).
- [5] R. H. Jansen et al., "High efficiency megawatt motor preliminary design," in *2019 AIAA/IEEE Electric Aircraft Technologies Symposium (EATS)*, Indianapolis, IN, USA, 2019, pp. 1-13, doi: [10.2514/6.2019-4513](https://doi.org/10.2514/6.2019-4513).
- [6] Y. Terao, W. Kong, H. Ohsaki, H. Oyori, and N. Morioka, "Electromagnetic Design of Superconducting Synchronous Motors for Electric Aircraft Propulsion," *IEEE Trans. Appl. Supercond.*, vol. 28, no. 4, pp. 1–5, Jun. 2018, doi: [10.1109/TASC.2018.2823503](https://doi.org/10.1109/TASC.2018.2823503).
- [7] M. Corduan, M. Boll, R. Bause, M. P. Oomen, M. Filipenko, and M. Noe, "Topology Comparison of Superconducting AC Machines for Hybrid Electric Aircraft," *IEEE Trans. Appl. Supercond.*, vol. 30, no. 2, pp. 1–10, Mar. 2020, doi: [10.1109/TASC.2019.2963396](https://doi.org/10.1109/TASC.2019.2963396).
- [8] R. C. Bolam, Y. Vagapov, and A. Anuchin, "A Review of Electrical Motor Topologies for Aircraft Propulsion," in *2020 55th International Universities Power Engineering Conference (UPEC)*, Torino, Italy, Sep. 2020, pp. 1–6. doi: [10.1109/UPEC49904.2020.9209783](https://doi.org/10.1109/UPEC49904.2020.9209783).
- [9] ASUMED, Final stakeholder report on project results, [online] Available: <https://cordis.europa.eu/project/id/723119/results>.
- [10] James L. Felder, NASA N3-X with Turboelectric Distributed Propulsion, <https://ntrs.nasa.gov/api/citations/20150002081/downloads/20150002081.pdf>
- [11] Konstantin L. Kovalev, Nickolay S. Ivanov, Superconducting Electric Machines for Future Electric Aircraft, in *The 4th International Symposium on More Electric Aircraft Technology*, Beijing, China, 2017.
- [12] R. H. Jansen, D. C. Bowman, A. Jankovsky, D. R. Dyson, and J. Felder, "Overview of NASA Electrified Aircraft Propulsion Research for Large Subsonic Transports", NASA Glenn Research Center, Cleveland, Ohio, US, Report Number ARC-E-DAA-TN49025, 2017.
- [13] Frank Anton, eAircraft: Hybrid-elektrische Antriebe fuer Luftfahrzeuge, [online] Available: <https://docslib.org/doc/752505/siemens-eaircraft-overview>.
- [14] E. Pardo, F. Grilli, Y. Liu, S. Wolfädler and T. Reis, "AC loss modeling in superconducting coils and motors with parallel tapes as conductor," *IEEE Transactions on Applied Superconductivity*, vol. 29, no. 5, pp. 1-5, Aug. 2019, Art no. 5202505, doi: [10.1109/TASC.2019.2899148](https://doi.org/10.1109/TASC.2019.2899148).
- [15] Y. Liu et al., "Investigation of AC loss of superconducting field coils in a double-stator superconducting flux modulation generator by using T-A formulation based finite element method," *Supercond. Sci. Technol.*, vol. 34, no. 5, p. 055009, May 2021, doi: [10.1088/1361-6668/abef7e](https://doi.org/10.1088/1361-6668/abef7e).
- [16] Y. Liu et al., "Comparison of 2D simulation models to estimate the critical current of a coated superconducting coil," *Superconductor Science and Technology*, vol. 32, no. 1, p. 014001, Nov. 2018, doi: [10.1088/1361-6668/aae960](https://doi.org/10.1088/1361-6668/aae960).
- [17] Y. Zhang, D. Zhou, T. Ida, M. Miki, and M. Izumi, "Melt-growth bulk superconductors and application to an axial-gap-type rotating machine," *Supercond. Sci. Technol.*, vol. 29, no. 4, p. 044005, Apr. 2016, doi: [10.1088/0953-2048/29/4/044005](https://doi.org/10.1088/0953-2048/29/4/044005).
- [18] K. Tsuzuki et al., "Design of Bulk HTS Rotating Machine Using Closed-Circuit Magnetization," *IEEE Trans. Appl. Supercond.*, vol. 29, no. 5, pp. 1–5, Aug. 2019, doi: [10.1109/TASC.2019.2902427](https://doi.org/10.1109/TASC.2019.2902427).
- [19] A. Patel, V. Climente-Alarcon, A. Baskys, B. A. Glowacki, and T. Reis, "Design considerations for fully superconducting synchronous motors aimed at future electric aircraft," in *2018 IEEE International Conference on Electrical Systems for Aircraft, Railway, Ship Propulsion and Road Vehicles & International Transportation Electrification Conference (ESARS-ITEC)*, Nottingham, Nov. 2018, pp. 1–6. doi: [10.1109/ESARS-ITEC.2018.8607734](https://doi.org/10.1109/ESARS-ITEC.2018.8607734).
- [20] F. Grilli et al., "Superconducting motors for aircraft propulsion: the Advanced Superconducting Motor Experimental Demonstrator project," *J. Phys.: Conf. Ser.*, vol. 1590, no. 1, p. 012051, Jul. 2020, doi: [10.1088/1742-6596/1590/1/012051](https://doi.org/10.1088/1742-6596/1590/1/012051).
- [21] N. Arish, F. Marignetti, and M. Yazdani-Asrami, "Comparative study of a new structure of HTS-bulk axial flux-switching machine," *Physica C: Superconductivity and its Applications*, vol. 584, p. 1353854, May 2021, doi: [10.1016/j.physc.2021.1353854](https://doi.org/10.1016/j.physc.2021.1353854).
- [22] M. Yazdani-Asrami, M. Zhang, and W. Yuan, "Challenges for developing high temperature superconducting ring magnets for rotating electric machine applications in future electric aircrafts," *Journal of Magnetism and Magnetic Materials*, vol. 522, p. 167543, Mar. 2021, doi: [10.1016/j.jmmm.2020.167543](https://doi.org/10.1016/j.jmmm.2020.167543).
- [23] J. H. Durrell et al., "Bulk superconductors: a roadmap to applications," *Supercond. Sci. Technol.*, vol. 31, no. 10, p. 103501, Oct. 2018, doi: [10.1088/1361-6668/aad7ce](https://doi.org/10.1088/1361-6668/aad7ce).
- [24] M. Kapolka et al., "Cross-field demagnetization of stacks of tapes: 3D modelling and measurements," *Supercond. Sci. Technol.*, Nov. 2019, doi: [10.1088/1361-6668/ab5aca](https://doi.org/10.1088/1361-6668/ab5aca).
- [25] T. Arndt et al., "New coil configurations with 2G-HTS and benefits for applications," *Supercond. Sci. Technol.*, vol. 34, no. 9, p. 095006, Sep. 2021, doi: [10.1088/1361-6668/ac19f4](https://doi.org/10.1088/1361-6668/ac19f4).
- [26] M. Sugano, T. Nakamura, K. Shikimachi, N. Hirano, and S. Nagaya, "Stress Tolerance and Fracture Mechanism of Solder Joint of YBCO Coated Conductors," *IEEE Transactions on Applied Superconductivity*, vol. 17, no. 2, pp. 3067–3070, Jun. 2007, doi: [10.1109/TASC.2007.899395](https://doi.org/10.1109/TASC.2007.899395).
- [27] Y. Tsui, E. Surrey, and D. Hampshire, "Soldered joints—an essential component of demountable high temperature superconducting fusion magnets," *Supercond. Sci. Technol.*, vol. 29, no. 7, p. 075005, Jul. 2016, doi: [10.1088/0953-2048/29/7/075005](https://doi.org/10.1088/0953-2048/29/7/075005).

- [28] Y. Wang, "Design, Analysis, and Experimental Test of a Segmented-Rotor High-Temperature Superconducting Flux-Switching Generator with Stationary Seal," *IEEE Transactions on Industrial Electronics*, vol. PP, Mar. 2018, doi: [10.1109/TIE.2018.2814001](https://doi.org/10.1109/TIE.2018.2814001).
- [29] F. Berg, J. Palmer, L. Bertola, P. Miller, and G. Dodds, "Cryogenic system options for a superconducting aircraft propulsion system," *IOP Conf. Ser.: Mater. Sci. Eng.*, vol. 101, p. 012085, Dec. 2015, doi: [10.1088/1757-899X/101/1/012085](https://doi.org/10.1088/1757-899X/101/1/012085).